Optical Gain and Saturation Considerations of Organic Dyes

W. Heudorfer

Institut für Theoretische Physik der Universität Stuttgart,
D-7000 Stuttgart-Vaihingen, Fed. Rep. Germany

G. Marowsky

Max-Planck-Institut für biophysikalische Chemie, Abteilung Laserphysik,
D-3400 Göttingen, Fed. Rep. Germany

F. K. Tittel

Department of Electrical Engineering, Rice University, Houston, Texas 77001, USA

Z. Naturforsch. **33a**, 1062–1068 (1978); received April 26, 1978

A theoretical analysis of optical gain and saturation of organic dye lasers is presented. An analysis based on a solution of the laser rate equations establishes a convenient method of optical gain measurement by internal fluorescence probing for low-gain systems, such as vapors of organic dyes. The concomitant limitations of high-gain systems (e.g. organic dyes in liquid solutions) of small-signal gain due to amplified spontaneous emission (ASE) and problems associated with gain saturation at high signal inputs are discussed in detail.

I. Introduction

Optical gain studies are essential in the development and analysis of new laser systems. Furthermore the determination of laser parameters which influence the gain characteristics such as excited state absorption [1, 2] is important in calculations predicting laser performance. Gain measurements for cw laser systems are relatively easy using a probe beam technique, but become more difficult for pulsed systems on account of synchronization and signal detection problems [3]. An elegant technique to overcome these experimental difficulties was first proposed by Sylfast [4]. This method involves a comparison of the fluorescence yield of various lengths of active medium. This method as developed so far is only applicable to low gain conditions. However, frequently even amplified spontaneous emission in the absence of optical cavity feedback may saturate the optical gain. In gain measurements of electron beam pumped argon-nitrogen laser mixtures Bhaumik [5] observed such saturation behaviour. In this paper we address ourselves first to a derivation of optical gain based upon a rate equation formulation, establishing a theoretical derivation for optical gain measurement by internal fluorescence probing. This general approach allows us in the second section of this paper to discuss the problems associated with lowering the small signal gain by intense amplification of spontaneous emission (ASE) for high-gain media. A theoretical description of gain saturation is included, in particular in terms of intensity and length of active medium dependence. Finally we present numerical data obtained for the example of a rhodamine 6G dye laser transversely pumped by a N_2-laser.

Reprint requests to Dr. G. Marowsky, Max-Planck-Institut für Biophysikalische Chemie, Karl-Friedrich-Bonhoeffer-Institut, Abteilung Laserphysik, Postfach 968, D-3400 Göttingen-Nikolausberg.

II. Basic Assumptions and Pumping Geometry

To study the amplification of an organic dye in liquid solution or in the gas phase we chose as pumping geometry transverse excitation of a cylindrical volume of length L_0 and diameter $2r_1$ with $2r_1 \ll L_0$. After homogeneous excitation by optical pumping or electron-impact induced collisional pumping [6] the dye molecules decay spontaneously with an isotropic distribution of the emitted fluorescence radiation. The spectral width is influenced by the concentration-dependent interaction between fluorescence and reabsorption [7]. Due to the pencil-like geometry of the active volume stimulated processes along the cylinder axis are favored against stimulation in direction of the excitation source. This behaviour allows us to approximate the three dimensional processes with a one dimensional model and a geometrical factor taking into consideration primarily those stimulated quanta traveling along the cylinder axis, similar to the assumptions of Reference [8] and [9]. However, only part of the radiation penetrating through one of the end faces of the active volume hits the detector located in a distance D (cf. Figure 1). This

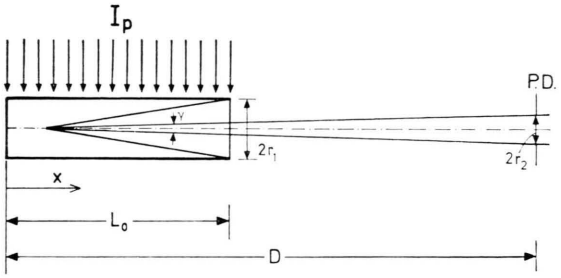

Fig. 1. Transverse pumping geometry. I_p: incident excitation intensity, D: position of photodiode (P.D.), L_0: length of the active medium.

fraction will depend on the spatially varying solid angle $\gamma(x) \cong \arctan(2r_2/(D-x))$.

Let us denote by $g_1^+(x)$ the probability that a spontaneously emitted light quantum at point x penetrates through the right cylinder face:

$$g_1^+(x) = \frac{1}{2}\left(1 - \frac{L_0 - x}{\sqrt{(L_0 - x)^2 + r_1^2}}\right) \tag{2.1}$$

similar for penetration through the lefthand side:

$$g_1^-(x) = \frac{1}{2}\left(1 - \frac{x}{\sqrt{x^2 + r_1^2}}\right). \tag{2.2}$$

The probability for hitting the detector will be:

$$g_2^+(x) = \frac{1}{2}\left(1 - \frac{D - x}{\sqrt{(D - x)^2 + r_2^2}}\right). \tag{2.3}$$

III. Rate Equations

The set of rate equations used in this contribution follows the formulation of Ganiel et al. [8] with additional consideration of excited state absorption [1, 2]. We denote with $J_1^+(x, t, \lambda)$ the spectral intensity traveling along the $+x$-direction and leaving the active volume at the righthand side, with $J_1^-(x, t, \lambda)$ the spectral intensity traveling in the opposite direction. The fraction $J_2^+(x, t, \lambda)$ is collected by the detector in the distance D.

$$\frac{1}{c}\frac{\partial}{\partial t} J_{1,2}^{\pm}(x, t, \lambda) \pm \frac{\partial}{\partial x} J_{1,2}^{\pm}(x, t, \lambda) = g_{1,2}^{\pm}(x)\frac{1}{\tau_1} \cdot E(\lambda) N_1 + J_{1,2}^{\pm}(x, t, \lambda)\,[\hat{\sigma}_e(\lambda) N_1 - \hat{\sigma}_{al}^1(\lambda) N_1 - \hat{\sigma}_{al}^0(\lambda) N_0 - \hat{\sigma}_{al}^t(\lambda) N_t], \tag{3.1}$$

$$\frac{\partial}{\partial t} N_1(x, t) = \sigma_{ap}^0 N_0 I_p - \frac{N_1}{\tau_1} + N_0 \int_{\text{band}} \hat{\sigma}_{al}^0(\lambda) J_1(x, t, \lambda)\,d\lambda - N_1 \int_{\text{band}} \hat{\sigma}_e J_1(x, t, \lambda)\,d\lambda. \tag{3.2}$$

The integrals of Eq. (3.2) denote the influence of amplified spontaneous emission (ASE) on the population of the excited state $S_1 \cdot N_0 \int_{\text{band}} \cdots$ is the additional pumping source via reabsorption and $-N_1 \int_{\text{band}} \cdots$ depicts stimulated emission via ASE. Even when considering J_2^+, the spectral intensity recorded with the fluorescence detector, we assume that the inversion N_1 is influenced by the total ASE-field, described by J_1 inside the active volume.

$$\frac{\partial}{\partial t} N_t(x, t) = k_{ST} N_1 - \frac{N_t}{\tau_t}, \tag{3.3}$$

$$N_{tot} = N_0 + N_1 + N_t, \tag{3.4}$$

$$J_1(x, t, \lambda) = J_1^+(x, t, \lambda) + J_1^-(x, t, \lambda). \tag{3.5}$$

The spectral quantum efficiency $E(\lambda)$ is related to the (total) quantum efficiency Φ by

$$\Phi = \int_{\text{band}} E(\lambda)\,d\lambda \tag{3.6}$$

with

$$E(\lambda) = 8\pi c\,\tau_1\,\hat{\sigma}_e(\lambda)\,\lambda^{-4}, \tag{3.7}$$

where c is the velocity of light and τ_1 the fluorescence lifetime of S_1. For the definition of the other quantities of equations (3.1)—(3.4) the reader is referred to Ref. [2] with the exception that $\hat{\sigma}_i$ corresponds to a wavelength dependent cross section $\hat{\sigma}_i = \hat{\sigma}_i(\lambda)$.

To facilitate the mathematical handling of the equations, an integration over the wavelength λ is performed:

$$I_{1,2}^{\pm}(x, t) = \int_{\text{band}} J_{1,2}^{\pm}(x, t, \lambda)\,d\lambda. \tag{3.8}$$

By definition of wavelength averaged cross sections $\bar{\sigma}_i$, the occurring convolution integrals are eliminated:

$$\bar{\sigma}_i = \frac{\int \hat{\sigma}_i(\lambda) J_{1,2}^{\pm}(x, t, \lambda)\,d\lambda}{\int J_{1,2}^{\pm}(x, t, \lambda)\,d\lambda}, \tag{3.9}$$

with the assumption of intensity-independent cross sections $\bar{\sigma}_i$ as defined by Equation (3.1).

Equations (3.1) and (3.2) yield:

$$\frac{1}{c}\frac{\partial}{\partial t} I_{1,2}^{\pm}(x, t) \pm \frac{\partial}{\partial x} I_{1,2}^{\pm}(x, t) = g_{1,2}^{\pm}(x)\frac{1}{\tau_1}\Phi N_1 + I_{1,2}^{\pm}(x, t)\,[\bar{\sigma}_e N_1 - \bar{\sigma}_{al}^1 N_1 - \bar{\sigma}_{al}^0 N_0 - \bar{\sigma}_{al}^t N_t], \tag{3.10}$$

$$\frac{\partial}{\partial t} N_1(x, t) = \sigma_{ap}^0 N_0 I_p - \frac{N_1}{\tau_1} + N_0 \bar{\sigma}_{al}^0 I_1 - N_1 \bar{\sigma}_e I_1, \tag{3.11a}$$

$$I_1 = I_1^+ + I_1^-. \tag{3.12}$$

An additional probe beam of intensity I_l^+ and wavelength λ_0 propagating in the $+x$-direction may be considered by:

$$\frac{1}{c}\frac{\partial}{\partial t} I_l^+(x,t) + \frac{\partial}{\partial x} I_l^+(x,t) = I_l^+[\sigma_e(\lambda_0) N_1 - \sigma_{al}^1(\lambda_0) N_1 - \sigma_{al}^0 N_0 - \sigma_{al}^t(\lambda_0) N_t], \tag{3.12}$$

$$\frac{\partial}{\partial t} N_1(x,t) = \sigma_{ap}^0 N_0 I_p - \frac{N_1}{\tau_1} + N_0(\bar{\sigma}_{al}^0 I_1 + \sigma_{al}^0 I_l^+) - N_1(\bar{\sigma}_e I_1 + \sigma_e I_l^+). \tag{3.11b}$$

IV. Gain without an External Input Signal ($I_l^+ = 0$)

a) Stationary Solutions

Equations (3.3), (3.4), (3.10), and (3.11) yield under stationary conditions ($\partial/\partial t = 0$):

$$\frac{\mathrm{d}}{\mathrm{d}x} I_{1,2}^{\pm}(x) = \pm g_{1,2}^{\pm}(x)\, \Phi\, N_1\, \tau_1^{-1} \pm I_{1,2}^{\pm}(x)[\bar{\sigma}_a N_1 - \bar{\sigma}_{al}^0 N_{tot}], \tag{4.1}$$

$$N_1(x) = \frac{N_{tot}(\sigma_{ap}^0 I_p + \sigma_{al}^0 I_1)\tau_1}{1 + (1 + k_{ST}\tau_t)\sigma_{ap}^0 \tau_1 I_p + [\bar{\sigma}_e + (1 + k_{ST}\tau_t)\bar{\sigma}_{al}^0]\tau_1 I_1}, \tag{4.2}$$

$$N_t = k_{ST}\tau_t N_1, \tag{4.3}$$

$$\bar{\sigma}_a = \bar{\sigma}_e - \bar{\sigma}_{al}^0 - \bar{\sigma}_{al}^0 k_{ST}\tau_t + \bar{\sigma}_{al}^0(1 + k_{ST}\tau_t), \tag{4.4}$$

$$\bar{\sigma}_a = \bar{\sigma}_{ef} + \bar{\sigma}_{al}^0(1 + k_{ST}\tau_t). \tag{4.4a}$$

The mathematical procedure will be to solve first (4.1) and (4.2) for $I_1^{\pm}(x)$ and determine $N_1(x)$. Another integration of (4.1) yields the unknown quantity $I_2^+(x)$.

b) Closed-form Solutions

In general the set of Eqs. (4.1)—(4.4) cannot be solved in closed form. However, there exists the interesting approximation of neglecting I_1 in Equation (4.2). This means that we allow ASE to be generated under the restriction of an intensity-independent inversion N_1 with $N_1 \neq N_1(x)$.

$$\frac{\mathrm{d}}{\mathrm{d}x} I_2^+(x) = g_2^+(x)\, \Phi\, N_1\, \tau_1^{-1} + I_2^+(x)[\bar{\sigma}_a N_1 - \bar{\sigma}_{al}^0 N_{tot}], \tag{4.5}$$

$$N_1 = \frac{N_{tot}\sigma_{ap}^0 \tau_1 I_p}{1 + (1 + k_{ST}\tau_t)\sigma_{ap}^0 \tau_1 I_p}. \tag{4.6}$$

For $D \gg L_0$ and $2r_2 \ll D$, $g_2^+(x)$ can be considered independent from x:

$$g_2^+ = \frac{1}{2}\left(1 - \frac{D - L_0/2}{[(D - L_0/2)^2 + r_2^2]^{1/2}}\right).$$

Equation (4.5) results in a first order differential equation with constant coefficients:

$$\frac{\mathrm{d}}{\mathrm{d}x} I_2^+(x) = \varkappa + (\alpha - \beta) I_2^+ \tag{4.7}$$

with

$$\alpha \equiv \bar{\sigma}_e N_1, \tag{4.8}$$

$$\beta \equiv \bar{\sigma}_{al}^0 N_{tot} - [\bar{\sigma}_{al}^0(1 + k_{ST}\tau_t) - \bar{\sigma}_{al}^1 - \bar{\sigma}_{al}^t k_{ST}\tau_t] N_1, \tag{4.9}$$

$$\varkappa \equiv \Phi\, g_2^+ N_1 \tau_1^{-1} \tag{4.10}$$

with N_1 given by (4.6), the definition of the net-gain $(\alpha - \beta)$ follows the notation of Reference [10] and [11]. Equation (4.9) essentially describes reabsorption of the stimulated radiation ($\beta \approx \bar{\sigma}_{al}^0 N_0$), modified by excited state and triplet state absorption.

A subdivision into three different cases of excitation lengths according to [4], [10], and [11] is now straightforward (see Figure 2):

a) Excitation of the total length:

$$I_2^+(1+2) = \frac{\varkappa}{\alpha - \beta}[e^{(\alpha-\beta)L_0} - 1]; \tag{4.11}$$

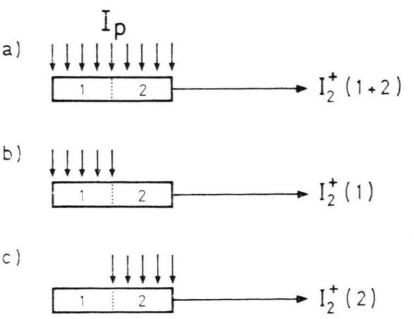

Fig. 2. Pumping geometry for gain probing via ASE, as discussed in Eqs. (4.11), (4.12), and (4.13).

b) Excitation of the lefthand side active volume:

$$I_2^+(1) = \frac{\varkappa e^{-\beta L_0/2}}{\alpha - \beta} [e^{(\alpha-\beta)L_0/2} - 1]; \qquad (4.12)$$

c) Excitation of the righthand side active volume:

$$I_2^+(2) = \frac{\varkappa}{\alpha - \beta} [e^{(\alpha-\beta)L_0/2} - 1]. \qquad (4.13)$$

Under these special conditions the equations for the unknown quantities α and β can separated and solved in a closed-form solution:

$$\alpha - \beta = \frac{2}{L_0} \ln \left[\frac{I_2^+(1+2)}{I_2^+(1)} - 1 \right] \qquad (4.14)$$

with

$$\beta = \frac{2}{L_0} \ln \left[\frac{I_2^+(2)}{I_2^+(1)} \right]. \qquad (4.15)$$

It is interesting to discuss to some extent the influence of the geometrical factor g_2^+. For simplicity let us assume the case $\alpha - \beta = 0$. Again neglecting the influence of ASE on N_1, we can now take into consideration the x-dependence of g_2^+ as defined in Equation (2.3). From Equation (4.5) results:

$$\frac{\mathrm{d}}{\mathrm{d}x} I_2^+(x) = g_2^+(x)\, \Phi\, N_1\, \tau_1^{-1}. \qquad (4.16)$$

Integration of this equation for case (a) and (c) leads to

$$\frac{I_2^+(1+2)}{I_2^+(2)} = \frac{L_0 + [(D-L_0)^2 + r_2^2]^{1/2} - (D^2 + r_2^2)^{1/2}}{L_0/2 + [(D-L_0)^2 + r_2^2]^{1/2} - [(D - L_0/2)^2 + r_2^2]^{1/2}}. \qquad (4.17)$$

For a typical experimental situation with $D = 20$ cm, $L_0 = 1.6$ cm, $r_0 = 0.05$ cm

$$I_2^+(1+2)/I_2^+(2) = 1.920001549. \qquad (4.17\,\mathrm{a})$$

A good approximation may be obtained by developing Eq. (4.17) for $r_0/D \ll 1$ and $L_0/D \ll 1$:

$$\frac{I_2^+(1+2)}{I_2^+(2)} \approx 2\left[1 - \frac{L_0}{2D}\left[1 - \frac{3}{4}\left(\frac{r_2}{D}\right)^2\right] + \cdots\right], \qquad (4.18)$$

$$I_2^+(1+2)/I_2^+(2) \cong 1.920001500. \qquad (4.18\,\mathrm{a})$$

Note that from Eq. (4.14) results for $\alpha - \beta = 0$

$$I_2^+(1+2)/I_2^+(2) = 2$$

upon setting $g_2^+ \neq g_2^+(x)$.

In order to show the influence of the above discussed approximations, Fig. 3 depicts a comparison of the pump intensity dependence of $(\alpha - \beta)$ for the closed-form solution (Eq. (4.14) and (4.15)) and a numerical integration of Eqs. (4.1) and (4.2). The following set of parameters has been chosen for the example of a N_2-laser pumped solution of the dye rhodamine 6G in methanol:

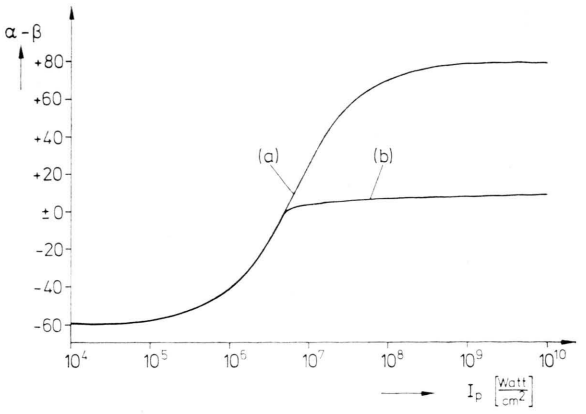

Fig. 3. Net-gain $(\alpha - \beta)$ versus pumping intensity I_p for a transversely excited solution of rhodamine 6G in ethanol (concentration $N_{tot} = 10^{18}$ cm^{-3}).
(a) Closed-form solution according Eq. (4.14) and (4.15) without ASE,
(b) numerical integration of Eq. (4.1) and (4.2) with inclusion of ASE.

$$\Phi = 1,$$
$$N_{tot} = 10^{18}\ \mathrm{cm}^{-3} \approx 1.33 \cdot 10^{-3}\ \mathrm{mol/liter},$$
$$\bar{\sigma}_{al}^0 = 0.6 \cdot 10^{-16}\ \mathrm{cm}^2 = \sigma_{al}^0,$$
$$\bar{\sigma}_e = 1.3 \cdot 10^{-16}\ \mathrm{cm}^2 = \sigma_e,$$
$$k_{ST}\, \tau_t = 0,$$
$$\bar{\sigma}_{al}^1 = 0.5 \cdot 10^{-16}\ \mathrm{cm}^2 \text{ (from Ref. [12])},$$
$$\tau_1 = 4\ \mathrm{ns}.$$

Curve (a) in Fig. 3 shows that the closed form solution with $N_1 + N_1(x)$ already reveals the saturation of $(\alpha - \beta)$ due to saturation of the transition by the pump intensity I_p. The result of additional numerical consideration of lowering of the inversion by $I_1^{\pm}$ is shown in curve (b) of Figure 3. In both cases the length L_0 has been chosen to $L_0 = 16$ mm, $D = 20$ cm (distance of the detector position) and $2r_2 = 1$ mm. The comparison clearly indicates the important role of ASE in mask-

ing the small-signal gain. The various saturation effects due to intense pumping I_p, large-signal input I_l and eventually ASE for high gain laser media are discussed in the subsequent section.

V. Input-Signal Amplification

In the general case of $I_l^+ \neq 0$ and $I_2^+ \neq 0$ the set of equations (3.10) for $I_1^\pm(x,t)$, (3.12) for $I_l^+(x,t)$ and Eqs. (3.11b), (3.3), and (3.4) have to be integrated to determine N_1, N_0, and N_t. Finally Eq. (3.10) yields the ASE-signal $I_2^+(x,t)$ in the presence of an external input signal I_l^+ $(x=0,t)$ and Eq. (3.12) yields the amplified signal I_l^+ $(x=L_0,t)$. Again we present numerical computer solutions under stationary conditions and compare these results with closed-form solutions for special assumptions.

a) Stationary Solution with I_l^+ and I_1^+

From Eqs. (3.11b), (3.3), and (3.4) follows:

$$N_1(x) = \frac{N_{tot}(\sigma_{ap}^0 I_p + \bar{\sigma}_{al}^0 I_1 + \sigma_{al}^0 I_l^+)\tau_1}{1 + (1 + k_{ST}\tau_t)\sigma_{ap}^0 \tau_1 I_p + [\cdots]\tau_1}, \tag{5.1}$$

$$[\cdots] = [\bar{\sigma}_e I_1 + \sigma_e I_l^+ + (1 + k_{ST}\tau_t) \cdot (\bar{\sigma}_{al}^0 I_1 + \sigma_{al}^0 I_l^+)],$$

$$\frac{d}{dx} I_{1,2}^\pm(x) = \pm g_{1,2}^\pm(x)\Phi N_1 \tau_1^{-1} \pm I_{1,2}^\pm(x)[\bar{\sigma}_a N_1 - \bar{\sigma}_{al} N_{tot}], \tag{5.2}$$

$$\frac{d}{dx} I_l^+(x) = I_l^+(\sigma_a N_1 - \sigma_{al}^0 N_{tot}). \tag{5.3}$$

It is convenient to recast Eq. (5.1) for $N_1(x)$ into an easier manageable expression by introduction of appropriate saturation intensities under the additional assumption:

$$I_1, I_l^+ \ll \frac{\sigma_{ap}^0}{\sigma_{al}^0} I_p,$$

$$I_{ps} = (\tau_1 \sigma_{ap}^0)^{-1},$$

$$I_{lS}^+ = \left(\sigma_e - \sigma_{al}^0 \frac{I_{ps}}{I_p}\right)^{-1} \tau_1^{-1}, \tag{5.1a}$$

$$I_{1S}^+ = \left(\bar{\sigma}_e - \bar{\sigma}_{al}^0 \frac{I_{ps}}{I_p}\right)^{-1} \tau_1^{-1},$$

$$N_1(x) = \frac{N_{tot} I_p / I_{ps}}{1 + (1 + k_{ST}\tau_t)\frac{I_p}{I_{ps}} + \frac{I_1}{I_{1S}} + \frac{I_l^+}{I_{lS}^+}}.$$

This equation clearly shows that the inversion is lowered by both, the ASE-signal I_1 normalized to its saturation signal I_{1S} and the input signal I_l^+ normalized to I_{lS}^+. In addition these saturation intensities exhibit the contribution of reabsorption via $\bar{\sigma}_{al}^0$ and σ_{al}^0 modified by the degree of saturation of the transition by optical pumping.

b) Stationary Solution with $I_l^+ \neq 0$ and $I_1^\pm = 0$

Whereas the problem of gain saturation of a traveling-wave amplifier at high signal input has already been discussed in elementary textbooks [13] for an ideal 4 level laser without reabsorption and triplet effects, there exists little information upon the influence of ASE, input signal light and excited state absorption on the gain of an optical amplifier. It turns out that ASE is of importance only for small signal inputs. Its apparent limitations of the detectivity of small signal amplification will be discussed with reference to a computer solution of Eq. (5.1)—(5.3) in Figure 4. As a con-

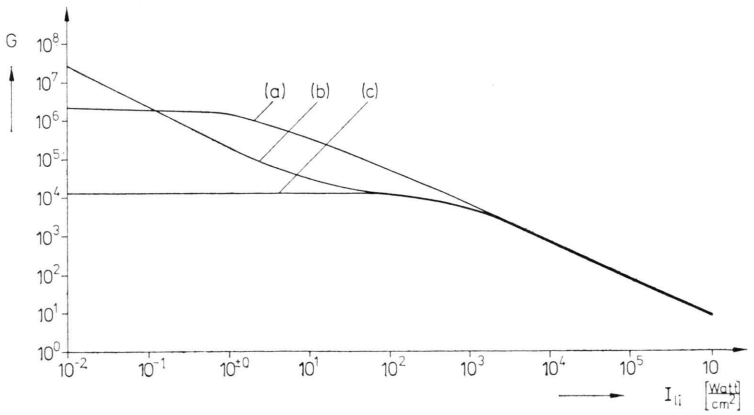

Fig. 4. Gain G versus intensity I_{li} of input signal for 3 different assumptions:

(a) $G_a = I_{lf}/I_{li}$ according Equation (5.12). Analytical solution without ASE,

(b) $G_b = (I_{lf} + I_2^+)/I_{li}$ according Eqs. (5.1), (5.2), and (5.3). Complete numerical solution with ASE.

(c) $G_c = I_{lf}/I_{li}$ according Eqs. (5.1), (5.2), and (5.3). Complete numerical solution with signal amplification G_c observed in the farfield to suppress ASE-contribution on observed output power.

$N_{tot} = 2 \cdot 10^{17}$ cm^{-3}, $I_p = 0.2 \cdot 10^8$ watt/cm^2, $\sigma_{ap}^0 = 2.3 \cdot 10^{-17}$ cm^2. Other laser parameters have been chosen as in Section IV b.

sequence of the nonlinear interaction of the various amplified signals, ASE can neglected at high input signals. However, the amplification and gain saturation behaviour will be essentially influenced by the coupling of excited state absorption via reabsoption, an effect not taken into account in Ref. [14] and [15], dealing with signal injection into a broadband amplifier. It is obvious that excited state absorption is of larger importance for an open amplifier as compared to a cavity laser, since the inversion $N_1(x)$ is no longer fixed to the steady state value required for the gain balancing the cavity losses.

For the sake of simplicity we neglect the factor $k_{ST}\tau_t$, assuming a quasi-stationary excitation of duration $\tau < k_{ST}^{-1}$ and $\tau > \tau_1$. The validity of the latter condition for a short-pulse N_2-laser excitation of only 2 ns duration will be discussed in detail in a subsequent paper [16].

With $I_1^{\pm} = 0$, Eqs. (5.1) and (5.3) yield:

$$\frac{\mathrm{d}}{\mathrm{d}x} I_l^+(x) = I_l^+ a_1 \frac{1 - a_3 I_l^+}{1 + a_2 I_l^+} \tag{5.4}$$

with

$$a_1 = \frac{\sigma_{ef}\tau_1 \sigma_{ap}^0 I_p - \sigma_{al}^0}{1 + \tau_1 \sigma_{ap}^0 I_p} N_{tot} \tag{5.5}$$

or with (5.1a)

$$a_1 = \frac{\sigma_{ef} I_p/I_{ps} - \sigma_{al}^0}{1 + I_p/I_{ps}}, \tag{5.6}$$

$$a_2 = \frac{(\sigma_e + \sigma_{al}^0)\tau_1}{1 + I_p/I_{ps}}, \tag{5.7}$$

$$a_3 = \frac{\sigma_{al}^0 \tau_1 \sigma_{al}^0}{\sigma_{ef} I_p/I_{ps} - \sigma_{al}^0}. \tag{5.8}$$

The quantity a_3 from Eq. (5.8) essentially describes the influence of excited state absorption (σ_{al}^1), coupled to I_l^+ via reabsorption (σ_{al}^0)*. Note that the closed-form solution of Eq. (5.4) changes its characteristics, if a_3 is neglected.

Let us define the amplification by

$$G \equiv I_{lf}^+/I_{li}^+ \tag{5.9}$$

and a small-signal amplification

$$\lim_{I_{li}^+ \to 0} G \equiv G_0 \equiv \exp(a_1 L_0) \tag{5.10}$$

* The modification of the effective fluorescence cross-sections by excited state absorption is included in σ_{ef}, cf. Eq. (4.4a).

with

$$B = a_2/a_3 = \frac{(\sigma_e + \sigma_{al}^0)(\sigma_{ef} I_p/I_{ps} - \sigma_{al}^0)}{(1 + I_p/I_{ps})\sigma_{al}^0 \sigma_{al}^0}. \tag{5.11}$$

Equation (5.4) can be integrated:

$$G_0 = G\left\{\left|\frac{1 - a_3 G I_{li}^+}{1 - a_3 I_{li}^+}\right|\right\}^{-(1+B)}. \tag{5.12}$$

The solution (5.12) contains some limiting cases of interest, requiring a separate discussion.

α) Small-signal limit ($I_{li}^+ \to 0$)

$$G = G_0 = e^{a_1 L_0} = \exp\left\{N_{tot} L_0 \frac{\sigma_{ef} I_p/I_{ps} - \sigma_{al}^0}{1 + I_p/I_{ps}}\right\}. \tag{5.13}$$

In the limit of $I_p \to 0$, Eq. (5.13) reduces to Beer's Law:

$$G = G_0 = \exp\{-N_{tot} L_0 \sigma_{al}^0\}. \tag{5.14}$$

The limit $I_p \gg I_{ps}$ yields the upper limit of amplification:

$$G \to \exp\{N_{tot} L_0 \sigma_{ef}\}. \tag{5.15}$$

β) Small-signal limit with $I_{li}^+ > 0$

with $I_S^{-1} = (G_0 - 1)(1 + B) a_3$ (5.16)

$$= (G_0 - 1)(a_2 + a_3). \tag{5.16a}$$

the lowering of the exponential small-signal gain G_0 can be described by

$$G = G_0(1 - I_{li}^+/I_S). \tag{5.17}$$

Let us discuss the quantitiy I_S which determines the onset of saturation, for the special case of $I_p \approx I_{ps}$ and $\sigma_e > \sigma_{al}^1 > \sigma_{al}^0$, a condition fulfilled for $\lambda > 560$ nm for rhodamine 6G according to Reference [12].

$$I_S^{-1} = \left\{\exp\left[N_{tot}\frac{L_0}{2}(\sigma_e - \sigma_{al}^0 - \sigma_{al}^1)\right] - 1\right\} \cdot \left\{\frac{\sigma_e + \sigma_{al}^0}{2} + \frac{\sigma_{al}^0 \sigma_{al}^1}{\sigma_e - \sigma_{al}^0 - \sigma_{al}^1}\right\}\tau_1. \tag{5.18}$$

Equation (5.18) clearly shows the various influences of reabsorption (σ_{al}^0) and excited state absorption (σ_{al}^1) of the signal light. A rigorous evaluation of Eq. (5.18) reveals the interesting effect that I_S increases with increasing σ_{al}^0 and σ_{al}^1. Hence the presence of reabsorption and excited state absorption delays the onset of gain saturation according

Eq. (5.17) due to an increase of the effective saturation intensity I_S.

In Fig. 4 is shown the dependence of the amplification $G = I_{lf}^{+}/I_{li}^{+}$ versus the input signal I_{li}^{+} for a N_2-laser pumped solution of rhodamine 6G in ethanol. The diagram indicates that an amplification of 10^4 can be obtained for not too large input signals, provided the signal light overcomes the ASE noise level. It is also apparent from this figure that the amount of ASE is lowered by an appropriate external signal input. This signal should comprise most of the excited active volume in order to avoid consumption of useful inversion by the adjacent ASE radiation.

Curve (a) of Fig. 4 depicts the saturation of the amplification by the increasing input signal I_{li}^{+}, using Eq. (5.12) in a closed form solution under neglection of ASE. Curve (b) shows the complete numerical result under inclusion of ASE by solution of Eqs. (5.1), (5.2), and (5.3). Since the quantity $G_b = (I_{lf} + I_2{}^{+})/I_{li}$ contains with the term $I_2{}^{+}$ the contribution of ASE on the total output signal, the (unphysical) increase of the amplification for very small input signals I_{lf} is reasonable. Curve (c) therefore indicates the dependence of G_c versus I_{li} in the far-field approximation: ASE is present in the active medium, lowers the available inversion but is not registered by the output detector located in the farfield. Note that the influence of ASE lowers the small-signal amplification by more than a factor of 200. At input intensities $I_{li} > 10^3$ watt/cm^2 gain saturation overcomes the influence of ASE due to the nonlinear interaction of I_{li} and $I_1{}^{\pm}$ on the effective inversion $N_1(x)$ according to Equation (5.1).

[1] O. Teschke, A. Dienes, and J. R. Whinnery, IEEE J. Quant. Electr. **QE-12**, 383 (1976).
[2] W. Heudorfer and G. Marowsky: In press in Appl. Physics.
[3] A. M. Hawryluk, J. A. Mangano, and J. H. Jacob, Appl. Phys. Lett. **31**, 164 (1977).
[4] W. T. Silfvast and J. S. Deech, Appl. Phys. Lett. **11**, 97 (1967).
[5] M. L. Bhaumik, Inst. Phys. Conf. Ser. **29**, 122 (1976).
[6] G. Marowsky, R. Cordray, F. K. Tittel, and W. L. Wilson, Appl. Phys. Lett. (in press).
[7] F. P. Schäfer (Ed.): Dye Lasers, 2nd ed., Topics in Applied Physics, Vol. 1, Springer-Verlag, New York 1977.
[8] U. Ganiel, A. Hardy, G. Neumann, and D. Treves; IEEE J. Quant. Electr. **QE-11**, 881 (1975).
[9] L. Allen and G. I. Peters: Phys. Rev. A 8, 2031 (1973).
[10] C. V. Shank, Rev. Mod. Phys. **47**, 649 (1975).
[11] P. W. Smith, P. F. Liao, C. V. Shank, C. Lin, and P. J. Maloney, IEEE J. Quant. Electr. **QE-11**, 84 (1975).
[12] E. Sahar and D. Treves: IEEE J. Quant. Electr. **QE-13**, 962 (1977).
[13] R. H. Pantell and H. E. Puthoff, Fundamentals of Quantum Electronics, John Wiley & Sons, New York 1969.
[14] P. Juramy, P. Flamant, and Y. H. Meyer, IEEE J. Quant. Electr. **QE-13**, 855 (1977).
[15] U. Ganiel, A. Hardy, and D. Treves, IEEE J. Quant. Electr. **QE-12**, 704 (1976).
[16] W. Heudorfer and G. Marowsky, to be published.

MINDO/3-FORCES Study of the $F^- + CH_4$ Reaction

Muthana Shanshal

Department of Chemistry, College of Science, University of Baghdad, Adhamiya, Baghdad, Iraq

Z. Naturforsch. **33a**, 1069–1071 (1978); received March 30, 1978

Using the MINDO/3-FORCES method the energy of the reactants, reaction products and the paths of reaction were calculated for $F^- + CH_4$. The calculated values of the cartesian force constants of five assumed structures showed that only the configuration of bipyramid (distorted C_{3v}) and the one with flourine bonded to a hydrogen atom are possible intermediates. Starting with the bipyramid the activation energy of the retention (63.6 kcal/mol) is calculated similar to the value recently reported for the same reaction of $H^- + CH_4$. We calculated also the activation energies for the inversion (56.4 kcal/mol), H_2 elimination (71.8 kcal/mol) and the proton abstraction (37.6 kcal/mol) reactions.

In the recent years the nucleophilic substitution reaction at the sp^3 hybridized C atom gained an increasing interest in the field of theoretical chemistry. Quantum mechanical calculations with different levels of approximation were carried out with the aim of studying this reaction [1–9]. In most of the reported calculations assumed geometries of the transition states and intermediates were considered. Thus for the reaction:

$$H^- + CH_4 \rightarrow CH_5^- \rightarrow CH_4 + H^- \qquad (1)$$

a D_{3h} transition state was accepted for the inversion reaction and a C_s transition state for the retention reaction [1, 2, 4, 5]. The activation energy of the inversion was calculated to be smaller than that of the retention reaction [2, 8, 9]. Reactions of methyl halides with nucleophilic agents were also studied [3, 6, 7, 8, 9]. It was found that nucleophilic reactions including the rupture of C–X bonds required smaller activation energies than those with C–H bond ruptures. Correlation energy effects were found small in the S_{N2} reaction [7].

Of considerable importance are still the following questions:

a) Whether the assumed D_{3h} (or C_{3v} for alkyl halide reactions) and C_s structures actually resemble the transition states of the inversion and retention reactions, respectively?

b) Whether the frequently discussed inversion and retention reactions are the only reactions caused by a nucleophilic attack and are not accompanied by other reactions such as the proton abstraction reaction

$$Y^- + X\text{-}CH_3 \rightarrow X\text{-}CH_2^- + Y\text{-}H\,, \qquad (2)$$

or elimination reactions of the type

$$Y^- + CH_4 \rightarrow Y\text{-}CH_2^- + H_2\,, \qquad (3)$$

$$Y^- + X\text{-}CH_3 \rightarrow Y\text{-}CH_2^- + X\text{-}H\,, \qquad (4)$$

or,

$$Y^- + X\text{-}CH_3 \rightarrow XY^- + CH_3\,. \qquad (5)$$

The latter reactions were predicted to be symmetrically allowed if the leaving atoms are coplanar [10]. In fact in recent molecular beam studies of the reaction of halogen ions with methane or methylhalides all these different ionic products have been observed [11]. It was also found that increasing the kinetic energy of the reactants increased and then decreased the reaction cross sections [11]. The formation of such products as XY^- may be atrributed to noninversion or retention steps or to secondary reactions following a primary process in which energetically high products are formed. To investigate the probability of the different reaction paths as well as the reasons for the change in the reaction cross sections we carrird out MINDO/3-FORCES [12] calculation for the reactants, reaction products and paths of the reaction

$$F^- + CH_4 \rightarrow \text{products}\,.$$

To start with we carried out the calculations for the structures of the frequently assumed transition states and intermediates shown in Figure 1.

It was found that out of the five calculated structures only (1) and (5) (Fig. 1) show thoroughly positive force constants and are therefore intermediates and not transition states of the reaction [13a]. The trigonal bipyramidal structure showed a distorted C_{3v} symmetry, the F is bent out of the z axis and the equatorial H atoms are slightly tilted out of the x-y plane towards the F atom. Similar light distortions had been calculated for the CH_5^- and $CH_3F_2^-$ ions [13b]. The prediction of these ions being intermediates agrees with former calculations

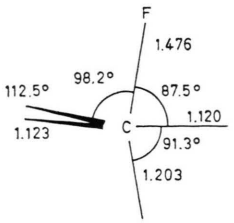

(1), $H_f = -48.75$ kcal/mol

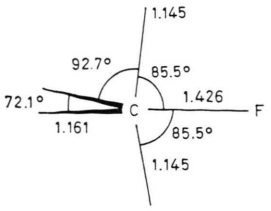

(2), $H_f = -41.98$ kcal/mol

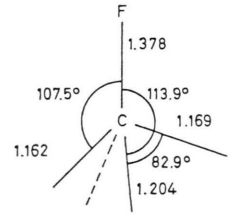

(3), $H_f = -15.87$ kcal/mol

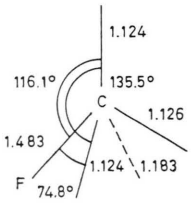

(4), $H_f = -45.77$ kcal/mol

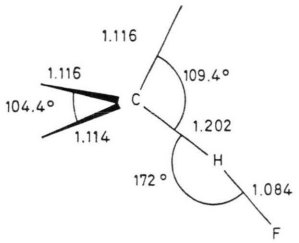

(5), $H_f = -58.64$ kcal/mol

Fig. 1. MINDO/3-FORCES calculated heats of formation and bond distances of assumed transition states and intermediates.

of the S_{N2} reaction [8b]. Using the MINDO/3 calculated heats of formation [14] for F^- (−41.33 kcal/mol), for CH_4 (−6.3 kcal/mol), and for H^- (60.01 kcal/mol) we calculated the following enthalpies of reactions:

		kcal/mol
$F^- + CH_4 \rightarrow$	$HCF^- + H_2 + H^\cdot$	127.38
	$H_3CF^- + H^\cdot$	58.29
	$H_3CF + H^-$	56.44
	$H_2CF^- + H_2$	50.70
	$H_3C^- + HF$	27.17

We calculated then the energies of the reacting system along the following paths:

a) The path of the inversion reaction with the C—H distance of the axial H atom leaving intermediate (1) as reaction coordinate,

b) The path of the retention reaction with the C—H distance of the equatorial H atom leaving intermediate (1) as reaction coordinate,

c) The path of the H_2 elimination reaction with both coplanar atoms departing from intermediate (1),

d) The path of the H—F elimination, beginning with intermediate (5), with the C—H distance of the abstracted H atom as reaction coordinate.

The energies of the system were minimized relative to all geometric parameters except the parameter resembling the reaction coordinate. This was kept constant during the calculation for each point along the reaction path. Figure 2 shows the calculated energy values for the system along the inversion, retention and H_2 elimination paths. Figure 3 shows the calculated energies along the abstraction reaction.

The calculated activation energies are:

inversion	56.4 kcal/mol (equivalent to the reaction enthalpy)
retention	63.6 kcal/mol
H_2 elimination	71.8 kcal/mol
H^+ abstraction	37.6 kcal/mol

The calculated activation energies of the retention and inversion reactions are comparable to those recently published [1—9]. Interesting is the low value for the H_2 elimination reaction. It suggests that this path should be convenient for systems with high kinetic energies of the reactants. It

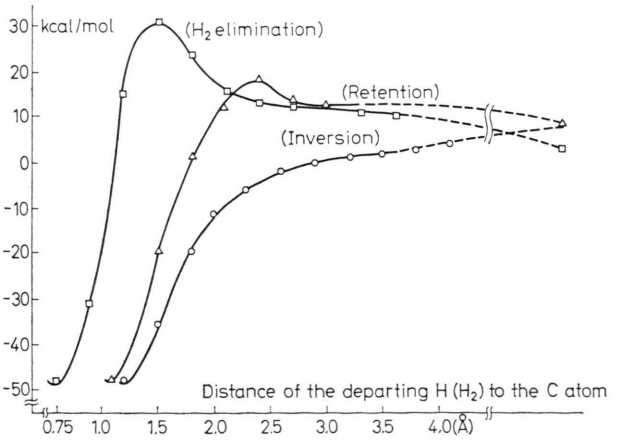

Fig. 2. MINDO/3-FORCES calculated reaction paths for the inversion, retention and H_2 elimination reactions of the $F^- + CH_4$ system.

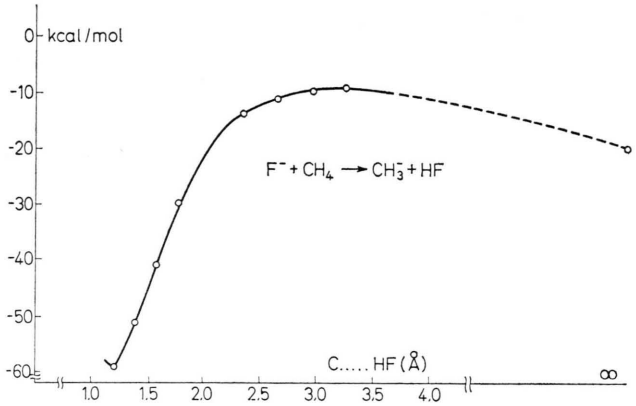

Fig. 3. MINDO/3-FORCES calculated reaction path for the H abstraction reaction of the $F^- + CH_4$ system.

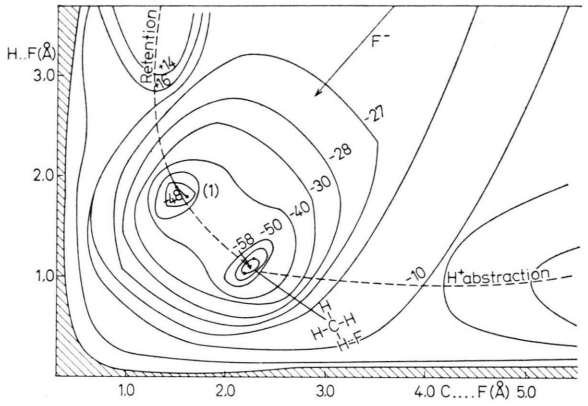

Fig. 4. MINDO/3-FORCES calculated hypersurface of $F^- + CH_4$ reaction with the intermediates (1) and (5).

provides an explanation for the formation of the ions H_2CX^- detected in molecular beam studies of reaction (3) [11]. A similar path might be responsible for the formation of H_2CX^-, X = Br or I, in the reaction [11]

$$X^- + H_3CF \rightarrow CH_2X^- + HF\,. \qquad (6)$$

No product of the H abstraction reaction (CH_3^-) could be detected in the $F^- + CH_4$ reaction [11]. This might be due to apparative reasons or to the high energy content of the initial halogen atoms which may cause a deviation of the reacting system from the hydrogen bonded intermediate (5). The hypersurface of the reaction system is shown in Figure 4. It is seen that the energy of $F^- + CH_4$ increases once F^- approaches methane. After this increase the energy decreases and the system goes to one of the two minima (1) and (5). Then the inversion, retention or H_2 elimination reactions proceed starting with intermediate (1). In Fig. 4 only the retention path could be drawn. The proton abstraction may proceed starting with intermediate (5). However the high energy content may cause a direct approach of the system to the product without passing through (1) or (5). Still, very high energy values may lead to an elastic collision of the system with the potential wall and a return to the initial state, $X^- + CH_4$, with no reaction occuring. This collision may explain the decline of the cross section curve on passing to the high kinetic energy values of the starting X^- ions [11].

Acknowledgement

The author thanks Prof. G. Stocklin, Jülich, for drawing his attention to this problem, Prof. H. Preuss, Stuttgart, Dr. E. Vietzke and G. Zellerman, Jülich for useful discussions. The MINDO/3-FORCES calculations were carried out at the Kernforschungs-Anlage Jülich.

[1] C. D. Ritchie and H. F. King, J. Amer. Chem. Soc. **90**, 838 (1968).
[2] W. Th. A. M. van der Lugt and P. Ross, Chem. Phys. Lett. **4**, 389 (1969).
[3] A. Dedieu and A. Veillard, Chem. Phys. Lett. **5**, 328 (1970).
[4] J. J. C. Mulder and J. S. Wright, Chem. Phys. Lett. **5**, 445 (1970).
[5] C. D. Ritchie and G. A. Chapelli, J. Amer. Soc. **92**, 1819 (1970).
[6] A. Dedieu and A. Veillard, J. Amer. Chem. Soc. **92**, 1819 (1970).
[7] F. Keil and R. Ahlrichs, J. Amer. Chem. Soc. **98**, 4787 (1976).
[8] W. D. Stohrer and K. R. Schneider, Chem. Ber. **109**, 285 (1976).
P. Gillespie, P. Hoffman, H. Klusacek, D. Marquarding, S. Pfogl, F. Ramirez, E. A. Tsolig, and I. Ugi, Angew. Chem. **83**, 691 (1971).
[9] H. B. Schlegel, K. Mislow, F. Bernardi, and A. Bottoni, Theor. Chim. Acta **44**, 245 (1977).
[10] R. Hoffman, J. Amer. Chem. Soc. **94**, 3047 (1972).
[11] N. Kashihira, E. Vietzke, and G. Zellerman, Chem. Phys. Lett. **39**, 316 (1976).
[12] S. M. Khalil and M. Shanshal, Theor. Chim. Acta **46**, 23 (1977).
[13] a) J. W. McIver Jr. and A. Komornicki, J. Amer. Chem. Soc. **94**, 2625 (1972). — b) M. Shanshal, unpublished work.
[14] R. C. Gingham, M. J. S. Dewar, and D. H. Lo, J. Amer. Chem. Soc. **97**, 1294 (1975); ibid **97**, 1307 (1975).